ARTICLES
PUBLISHED ONLINE: 14 MARCH 2016 | DOI: 10.1038/NCHEM.2475
nature chemistry

# A simple physical mechanism enables homeostasis in primitive cells

Aaron E. Engelhart[1†], Katarzyna P. Adamala[1,2†] and Jack W. Szostak[1*]

**The emergence of homeostatic mechanisms that enable maintenance of an intracellular steady state during growth was critical to the advent of cellular life. Here, we show that concentration-dependent reversible binding of short oligonucleotides, of both specific and random sequence, can modulate ribozyme activity. In both cases, catalysis is inhibited at high concentrations, and dilution activates the ribozyme via inhibitor dissociation, thus maintaining near-constant ribozyme specific activity throughout protocell growth. To mimic the result of RNA synthesis within non-growing protocells, we co-encapsulated high concentrations of ribozyme and oligonucleotides within fatty acid vesicles, and ribozyme activity was inhibited. Following vesicle growth, the resulting internal dilution produced ribozyme activation. This simple physical system enables a primitive homeostatic behaviour: the maintenance of constant ribozyme activity per unit volume during protocell volume changes. We suggest that such systems, wherein short oligonucleotides reversibly inhibit functional RNAs, could have preceded sophisticated modern RNA regulatory mechanisms, such as those involving miRNAs.**

Modern organisms employ a wide range of sophisticated homeostatic mechanisms to regulate their internal states in response to both internal and external fluctuations in conditions. The fact that modern homeostatic mechanisms use complex biochemical machinery raises the question of whether the earliest cells entirely lacked homeostatic processes, or whether intrinsic physical processes that conferred a degree of homeostasis were present from the beginning. Fatty acid vesicles—models of primitive cells—are dynamic systems that can grow in response to osmotic stress, the addition of fatty acid micelles and the activity of encapsulated catalysts[1–3]. One example of such a dynamic behaviour occurs in vesicles containing phospholipids or hydrophobic peptides, which can grow at the expense of surrounding vesicles that lack phospholipids or hydrophobic peptides[3–7]. Such abilities were probably critical elements of protocell fitness[7,8], but the increase in volume resulting from growth dilutes the encapsulated solutes, including catalysts such as ribozymes. The resulting decreased specific activity of cellular ribozymes would, in turn, have slowed RNA-catalysed RNA replication, metabolism and other cellular activities. Although the vesicle membrane itself has been used as a reaction promoter, suggesting a partial solution to increased requirements for catalysts resulting from cellular (and, thus, membrane) growth[3,9], it remains unclear how membrane growth could have been coupled to the regulation of catalytic function within the vesicle lumen. Here, we demonstrate a simple physical process that could have increased the activity of ribozyme catalysts within growing primordial cells, thus compensating for the volume changes resulting from cell growth. Our demonstration of enhanced enzyme activity as a result of growth-driven dilution of cellular contents, which results in approximately constant enzyme specific activity (on a volume basis) before and after vesicle growth-induced dilution, shows that simple physical homeostatic mechanisms could have been operative in the earliest cells.

We examined whether the growth of a vesicle membrane and concomitant dilution of its contents could result in the activation of a ribozyme catalyst by dissociation of short oligonucleotide inhibitors, such as those expected to be generated by random RNA synthesis, partial RNA copying reactions, or non-specific degradation of RNA. As a model functional RNA we employed the well-characterized hammerhead ribozyme. This enzyme can be assembled from two oligonucleotides, **HH-A** and **HH-B**. The resulting **HH-A/HH-B** complex catalyses the self-cleavage of **HH-A** (ref. 10). We first screened in solution a series of ten 5–7 nucleotide (nt) oligonucleotide inhibitors (**HH-I-1** to **HH-I-10**) that were complementary to sequences within **HH-B**, by measuring cleavage yield after overnight incubation at saturating $Mg^{2+}$. These oligonucleotides had predicted dissociation constants for **HH-B** of between ~250 nM and 800 μM (Supplementary Table 1). We carried out reactions at three different concentrations, with the inhibitor oligonucleotide present in 100-fold excess relative to **HH-A** and **HH-B**, which were present at 0.1–10 μM each. We reasoned that, at high concentration, these relatively weakly binding oligonucleotides would inhibit the formation of the active **HH-A/HH-B** ribozyme complex (Fig. 1); following dilution, they would dissociate, allowing reconstitution of the functional ribozyme. Only the tightest-binding inhibitor, **HH-I-10**, exhibited significant (>50%) inhibition at high concentration (Supplementary Fig. 1); **HH-I-1** to **9** exhibited no significant inhibition of hammerhead activity. The addition of two more weakly binding inhibitors, **HH-I-3** and **HH-I-9**, enhanced the inhibition caused by **HH-I-10**, resulting in 98% suppression of ribozyme activity (as measured by overnight cleavage yield) at 10 μM enzyme concentration and 1 mM inhibitor concentration. However, 68% cleavage was observed on dilution to 0.1 μM enzyme and 10 μM inhibitor concentration (Supplementary Fig. 2). Interestingly, the weakly binding oligonucleotide **HH-I-3**, with a predicted dissociation constant of ~160 μM, is a significant contributor to the suppression of enzyme activity when used in systems containing **HH-I-10** as well (Supplementary Figs 2 and 3), demonstrating the importance of cooperative interactions in networks of interacting RNAs.

Having screened these inhibitors by endpoint analysis, we examined the reaction kinetics of ribozyme–inhibitor mixtures in more detail. The three-inhibitor **HH-I-3/9/10** system, as well as

[1]Department of Molecular Biology, and Center for Computational and Integrative Biology, Howard Hughes Medical Institute, Massachusetts General Hospital, Boston, Massachusetts 02114, USA. [2]MIT Media Lab, 77 Massachusetts Avenue, E14/E15, Cambridge, Massachusetts 02139-4307, USA; †These authors contributed equally to this work. *e-mail: szostak@molbio.mgh.harvard.edu

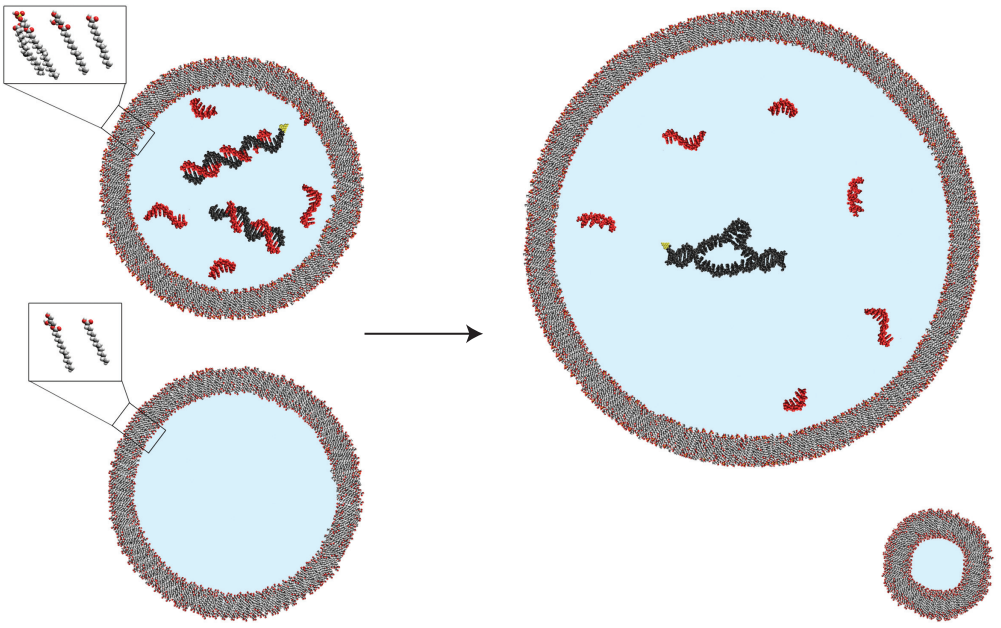

**Figure 1 | Regulation of enzyme activity in model protocells by dissociation of short complementary oligonucleotides.** Mixed fatty acid/glycerol ester/phospholipid vesicles that contain split ribozymes (black) and high concentrations of short oligonucleotides (red) exhibit no ribozyme activity, due to inhibition by duplex formation between the ribozyme fragments and complementary oligonucleotides (top left). When mixed with vesicles lacking phospholipid (bottom left), the phospholipid-containing vesicles grow at the expense of the phospholipid-lacking vesicles. This growth results in dilution of vesicle contents, inhibitor dissociation, and ribozyme reconstitution (right), increasing catalyst activity in the enlarged vesicles.

those containing each single inhibitor alone, exhibit kinetics consistent with the results above. At 10 μM **HH-A/HH-B** concentration, 1 mM each of **HH-I-3/9/10** results in a >100-fold reduction in apparent rate constant relative to the uninhibited **HH-A/HH-B** enzyme—a significantly greater reduction in rate than resulting from any single inhibitor (Fig. 2 and Supplementary Table 2). When this system is diluted 100-fold (to 100 nM ribozyme concentration), the weakly binding inhibitors dissociate, with the **HH-I-3/9/10** system exhibiting 53% of the apparent rate constant of the uninhibited **HH-A/HH-B** system at this concentration. The order of addition (inhibitors added to **HH-B** followed by **HH-A**, or inhibitors added to a pre-formed **HH-A/HH-B** complex) did not affect concentration-dependent ribozyme inhibition (Supplementary Fig. 4), suggesting that the active and inhibited complexes were in fast exchange.

We next sought to examine whether such interactions could be relevant to a system of model protocell vesicles composed of fatty acids and encapsulated RNAs. We employed a fatty acid vesicle system consisting of a 2:1 mixture of myristoleic acid and glycerol monomyristoleate (MA/GMO vesicles). This system was previously reported to be robust to at least 4 mM magnesium ($Mg^{2+}$) and is capable of supporting hammerhead ribozyme activity[11]. We have previously shown that oleate vesicles containing a small fraction of phospholipid grow when surrounded by pure oleate vesicles; this competitive growth is a result of the slower off-rate of fatty acid molecules from membranes that contain some phospholipid[7]. We therefore examined the 2:1 myristoleic acid:glycerol monomyristoleate vesicle system to see if it, too, would undergo competition-based growth when doped with a small amount (10 mol%) of diacylphospholipid (here, DOPA, or dioleylphosphatidic acid). When 2:1 MA/GMO vesicles containing 10 mol% DOPA (MA/GMO/DOPA vesicles) were mixed with 20 equiv. of pure MA/GMO vesicles, they grew in surface area approximately threefold (corresponding to a fivefold volume increase, given spherical vesicles, Supplementary Fig. 5); full volume relaxation occurred over ~3 h (Supplementary Fig. 6).

We examined hammerhead function in this vesicle system at 1 μM ribozyme, reasoning that an intermediate concentration of the **HH-A/HH-B/HH-I-3/9/10** system would be most sensitive to concentration changes. The **HH-A/HH-B** complex without inhibitors, encapsulated in MA/GMO/DOPA vesicles at 1 μM ribozyme concentration, exhibited an apparent rate constant for self-cleavage of 0.23 $h^{-1}$ (Fig. 3 and Supplementary Table 2), similar to the unencapsulated control. On mixing with 20 equiv. of MA/GMO vesicles and vesicle swelling (with concomitant dilution of contents), a rate depression to 0.11 $h^{-1}$ was observed, somewhat lower than that observed with unencapsulated ribozyme. This rate decrease is presumably a result of dissociation of the **HH-A/HH-B** complex, owing, in both cases, to the **HH-A/HH-B** concentration approaching the $K_d$ of hammerhead ribozymes of this stem length[10]. The overall lower rate in liposomes is probably a result of chelation of $Mg^{2+}$ by fatty acids.

Having validated hammerhead function in this system, we examined the kinetics of this enzyme in the presence of inhibitors. The presence of 100 μM each of **HH-I-3/9/10** in unswollen vesicles resulted in almost total abolition of 1 μM **HH-A/HH-B** ribozyme activity, with an intravesicle apparent rate constant of 11% of the uninhibited reaction (Fig. 3). The addition of 20 equiv. of MA/GMO vesicles to these vesicles and subsequent swelling and dilution of their contents resulted in reconstitution of ribozyme activity to an apparent rate constant of 0.12 $h^{-1}$—essentially identical to the uninhibited rate constant in vesicles after volume growth (Fig. 3 and Supplementary Table 2). Thus, the increased volume of the vesicle lumen following membrane growth resulted in ribozyme activation.

Encouraged by these results, we asked whether random oligonucleotides, such as those generated by untemplated synthesis, could exhibit a similar effect. Remarkably, in an unencapsulated system, the random oligonucleotide **r($N_6$)**, when present at 300 equiv. relative to **HH-A/HH-B**, suppressed catalytic activity to near-undetectable levels ($k_{app} < 0.005\ h^{-1}$) at 10 μM **HH-A/HH-B** concentration (3 mM **r($N_6$)**), with recovery to an apparent rate constant of 0.10 $h^{-1}$ on dilution to 0.1 μM **HH-A/HH-B** (30 μM **r($N_6$)**,

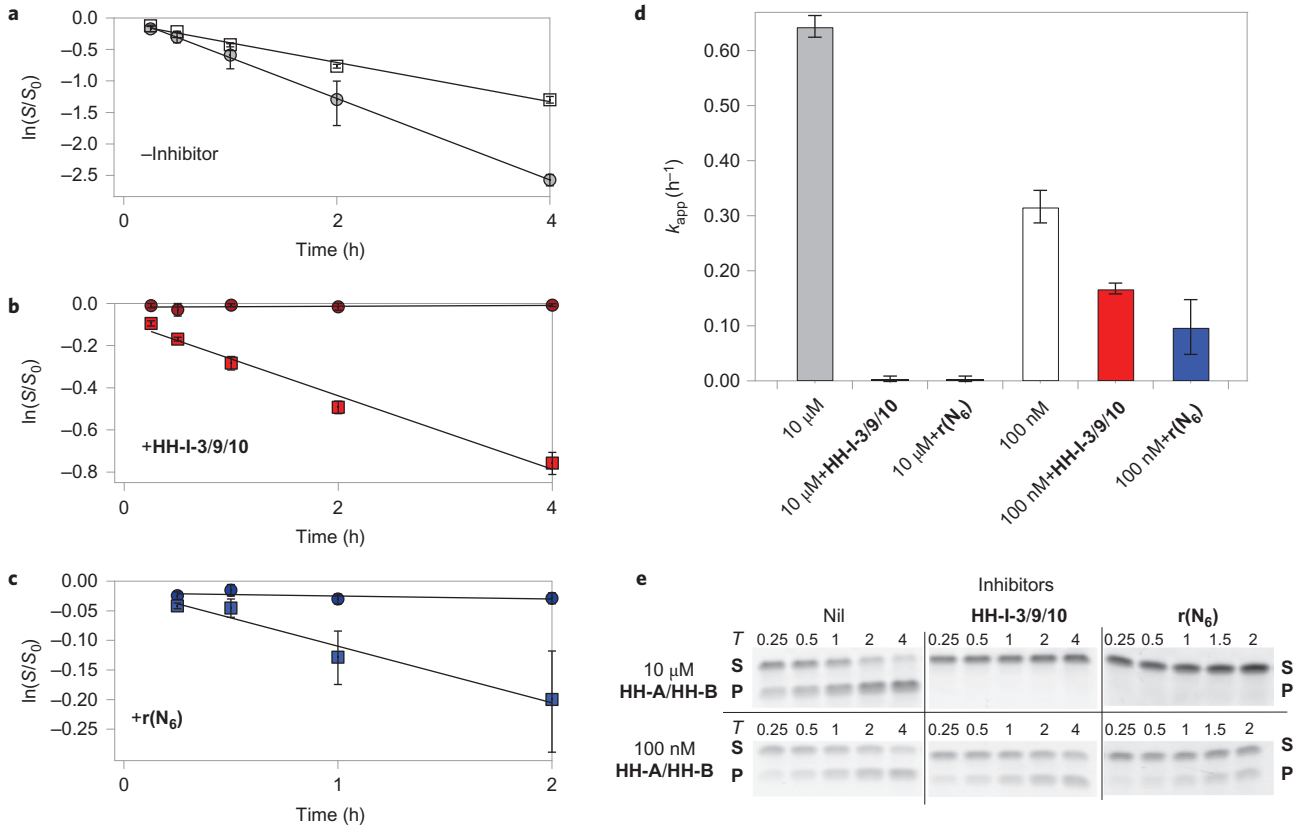


**Figure 2 | A small ribozyme exhibits diminished activity upon dilution, while the same ribozyme, in the presence of short oligonucleotide inhibitors, exhibits enhanced activity upon dilution. a–c**, Time courses of hammerhead ribozyme cleavage, expressed as natural log of remaining fraction of uncleaved **HH-A** versus time. In **a**, there are no inhibitors: white squares, 100 nM each **HH-A**/**HH-B**; grey circles, 10 μM each **HH-A**/**HH-B**. In **b**, **HH-I-3/9/10** inhibitor oligonucleotides are present: red squares, 100 nM each **HH-A**/**HH-B**, 10 μM each **HH-I-3/9/10** (not inhibited); dark red circles, 10 μM each **HH-A**/**HH-B**, 1 mM each **HH-I-3/9/10** (inhibited). In **c**, random-sequence inhibitor oligonucleotides **r(N$_6$)** are present: blue squares, 100 nM each **HH-A**/**HH-B**, 30 μM **r(N$_6$)** (not inhibited); dark blue circles, 10 μM each HH-A/HH-B, 3 mM **r(N$_6$)** (inhibited). Error bars represent s.e.m. of ribozyme cleavage product yields, $N = 3$. **d**, Rates of ribozyme cleavage in the conditions specified in **a–c**. Error bars represent s.e.m., $N = 3$. **e**, Representative polyacrylamide gel electrophoresis (PAGE) analyses of hammerhead ribozyme reactions. Substrate (**HH-A**) is denoted as **S** and cleavage product as **P**. Reaction time *T* in hours is given above each gel lane.

Supplementary Table 2). A mixture of 2 mM **r(N$_6$)** and 1 mM **r(N$_5$)** also exhibited concentration-dependent inhibition, with an apparent rate constant of 0.0057 h$^{-1}$ observed for 10 μM **HH-A/HH-B** (Supplementary Table 2); 100-fold dilution (to 0.1 μM **HH-A/HH-B**, 20 μM **r(N$_6$)**, 10 μM **r(N$_5$)**) gave an apparent rate constant of 0.17 h$^{-1}$. We examined each of these systems in MA/GMO/DOPA vesicles as before. In encapsulated systems containing 1 μM **HH-A/HH-B**, 300 equiv. (300 μM) **r(N$_6$)** gave an apparent rate constant of 0.027 h$^{-1}$, corresponding to 88% inhibition; a mixture of 200 equiv. **r(N$_6$)** and 100 equiv. **r(N$_5$)** gave an apparent rate constant of 0.043 h$^{-1}$, corresponding to 81% inhibition (Supplementary Table 2 and Fig. 3). Vesicle growth induced by the addition of 20 equiv. MA/GMO vesicles resulted in ribozyme reconstitution in both systems, with an apparent rate constant of 0.099 h$^{-1}$ for **r(N$_6$)** alone and 0.11 h$^{-1}$ for the mixed random-inhibitor system. These changes represent 3.7- and 2.6-fold increases in rate constant, in contrast to the approximately twofold decrease in the rate constant of the uninhibited **HH-A/HH-B** system upon vesicle growth. These results show that even a random-sequence pool of short oligonucleotides could have contributed to homeostatic behaviour in primitive cells. Given that the short RNA pool in an early cell would have exhibited at least partial sequence complementarity to longer RNAs, owing to templating effects and enhanced chemical stability of base-paired RNAs, we expect that the magnitude of these phenomena in primordial cells would be intermediate to those observed with the **HH-I-3/9/10** and **r(N$_6$)** inhibitor systems.

We have previously suggested that short oligonucleotides generated in primordial cells as a consequence of partial replication reactions could act as replication intermediates in a hierarchical template-copying process[12]. As it is likely that each copy of a functional RNA synthesized during replication is produced along with many partial copies[13–16], such short oligonucleotides were probably abundant in primitive cells. Here, we have demonstrated that such short oligonucleotides can also act as concentration-dependent ribozyme inhibitors. These inhibitors afford model protocell vesicles the ability to activate ribozymes following growth via competitive processes, as shown here, or by other, non-competitive mechanisms, such as the growth of vesicles following sporadic exposure to fatty acid micelles. Such concentration-dependent inhibition could, in turn, have led to simple homeostatic mechanisms that may have been functional in the earliest cells. For example, if a protocell contained ribozymes that contributed to RNA replication or metabolic reactions, concentration-dependent inhibition would tend to slow down RNA replication or metabolism when internal RNA concentrations were high, but RNA-based catalysts of replication or other metabolic processes would activate following cell growth, thus contributing to the maintenance of a constant internal environment. In our experiments, the specific activity of an encapsulated ribozyme following growth is only ~10% of that before growth (twofold loss of total activity due to strand dissociation, together with fivefold dilution; Supplementary Table 2). In contrast, for encapsulated ribozyme-inhibitor systems, the initial rate of product formation per unit

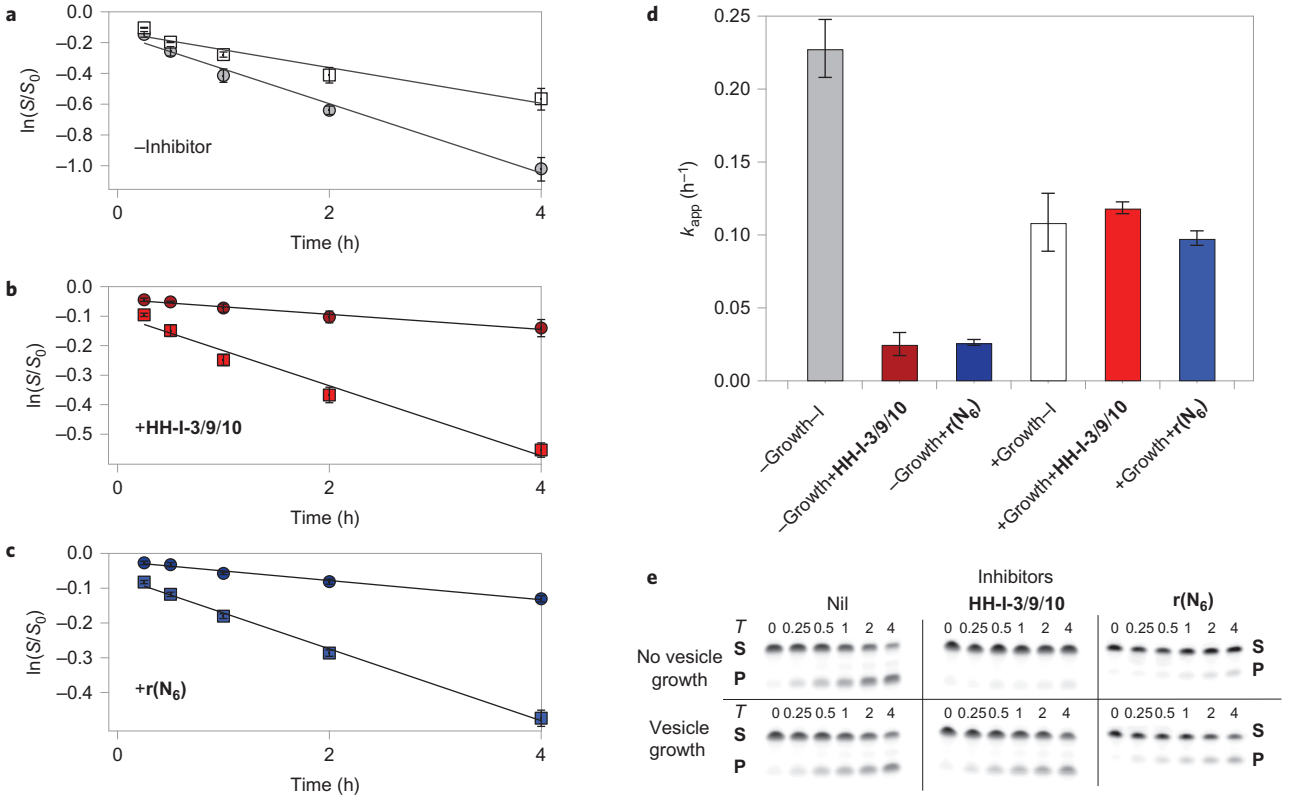


**Figure 3 | Competition-driven growth relieves inhibition of ribozyme activity in vesicles. a–c**, Time courses of hammerhead ribozyme cleavage, expressed as natural log of remaining fraction of uncleaved **HH-A**, versus time. All reactions were performed in MA/GMO/DOPA vesicles containing an initial concentration of 1 μM each **HH-A** and **HH-B** and 100 μM each **HH-I-3/9/10** or 300 μM **r(N$_6$)** (if inhibitors were present). Error bars represent s.e.m. of ribozyme cleavage product yields, $N = 4$. In **a**, there are no inhibitors: grey circles, no vesicle growth; white squares, vesicle growth induced by mixing with 20 equiv. (relative to lipid) MA/GMO vesicles. In **b**, **HH-I-3/9/10** inhibitor oligonucleotides are present: dark red circles, no vesicle growth; red squares, vesicle growth induced as above. In **c**, random-sequence inhibitor oligonucleotides **r(N$_6$)** are present: dark blue circles, no vesicle growth; blue squares, vesicle growth induced as above. **d**, Rates of ribozyme cleavage in the conditions specified in **a–c**. Error bars represent s.e.m., $N = 4$. **e**, Representative PAGE analyses of hammerhead ribozyme reactions. Substrate (**HH-A**) is denoted as **S** and cleavage product as **P**. Oligonucleotides of lengths spanning a range of those used were retained within swollen, $Mg^{2+}$-treated vesicles (Supplementary Fig. 10), demonstrating that the observed reaction occurs within vesicles. Reaction time *T* in hours is given above each gel lane.

volume after growth is ~50–100% of that before growth. These results suggest that the mechanisms we have described could have helped maintain a constant internal environment by regulating the activity of the ribozymes required for metabolic processes in growing cells (such as polymerases, proofreading enzymes and so on). Thus, the activation of catalysts in response to the dilution associated with cellular growth could have afforded one of the earliest means of maintaining intracellular homeostasis—a critical step in early cellular evolution. We speculate that the mechanism described here could have been elaborated through the evolution of increasingly finely tuned ribozyme inhibitors optimized for affinity and specificity, as well as increasingly sophisticated ribozymes enabling more complex cellular functions. The hammerhead ribozyme used here produces fragments that, themselves, could act as product inhibitors in multiple-turnover catalysis, with predicted dissociation constants on the order of $1 \times 10^{-9}$ and $1 \times 10^{-7}$ M (Supplementary Table 1). We note that robust multiple turnover is possible with this hammerhead construct[10], and any such product inhibition would be highly dependent on stem sequences. For example, the two stems found in the enzyme used in this work are both hexanucleotides, but they have predicted $K_D$ values differing by approximately two orders of magnitude. This suggests a simple means by which primitive nucleases could have evolved to regulate their capacity for multiple turnover catalysis.

The predicted yields of full-length functional RNAs and short inhibitors, based on stepwise coupling efficiencies (Supplementary Fig. 7 and Supplementary Table 3), suggest that inhibitor:functional RNA ratios similar to those in this work would arise naturally as a result of RNA synthesis processes with ~85% stepwise coupling efficiency. This lies within the range of coupling efficiencies observed for the most effective known ribozyme RNA polymerases[13,14]. Additionally, it is likely that trans-esterification-mediated degradation of unstructured RNAs helped contribute to the short RNA pool in primitive cells[15].

Such primitive RNA regulatory mechanisms could have contributed to the development of complex RNA-based cells and the ability of such cells to adapt to divergent and variable environments. Indeed, given the rich array of regulatory behaviours modulated by short non-coding RNAs in contemporary life[17], it is not surprising that an early form of life with primarily RNA-based catalysts might have exploited such phenomena. The mechanisms we have described here represent a primitive form of ncRNA-based regulation of cellular behaviour that may have been operative in the earliest forms of life.

## Methods

**Oligonucleotides.** All oligonucleotides were obtained from IDT. **HH-A** (r(fluorescein-CG CGC CGA AAC ACC GUG UCU CGA GC)) and **HH-B** (r(GGC UCG ACU GAU GAG GCG CG)) were obtained with HPLC purification. Random-sequence oligonucleotides **r(N$_6$)** (r(NNN NNN)) and **r(N$_5$)** (r(NNN NN)), **HH-I-1** to **HH-I-10**, and **FAM-DNA-HH-I-3** (d(Fluorescein-TC GAG), the fluorescently labelled DNA equivalent of **HH-I-3**) were obtained desalted but not

HPLC-purified. **r($N_6$)** and **r($N_5$)** were prepared by mix-on-machine delivery of all four RNA phosphoramidites in equimolar amounts. The affinities of **HH-I-1** to **HH-I-10** and the sequences comprising the 5′ and 3′ stems formed in the **HH-A/HH-B** complex, **HH-A-5pStem** and **HH-A-3pStem**, for **HH-B**, were calculated using MELTING 5.1.0 (Supplementary Table 1)[18,19].

**Lipids.** Myristoleic acid and glycerol monomyristoleate were obtained from Nu-Chek, dioleylphosphatidic acid (DOPA) was obtained from Avanti Polar Lipids and rhodamine DHPE (lissamine rhodamine B 1,2-dihexadecanoyl-*sn*-glycero-3-phosphoethanolamine) and NBD DHPE (NBD 1,2-dihexadecanoyl-*sn*-glycero-3-phosphoethanolamine) were from Life Technologies.

**Other materials.** Tris-HCl (1 M solution), $MgCl_2$ (1 M solution) and RNAse-free water (non-DEPC-treated; DEPC=diethylpyrocarbonate) were from Life Technologies. Hand-poured denaturing polyacrylamide gels (20%) were prepared using the UreaGel concentrate/diluent system from National Diagnostics. Pre-cast denaturing polyacrylamide gels (15%) were Novex TBE-urea gels from Life Technologies. TBE (in hand-poured gels and running buffer) was 1×, prepared from a 10× stock solution (0.89 M tris, 0.89 M boric acid, 0.01 M EDTA). Track-etched membranes for vesicle extrusion were Nucleopore brand from Whatman/GE. Other reagents and solvents were from Sigma, Fisher or VWR.

**Vesicles.** Thin films of lipids were prepared by drying a chloroform or dichloromethane solution of the desired final lipid composition in a glass vial under a stream of argon. The resulting film was resuspended in a solution of 250 mM tris-HCl pH 8 with 0.5 equiv. NaOH relative to unesterified carboxylic acid (myristoleic acid) and tumbled for 12–18 h, after which vesicles were sized and made unilamellar by nine extrusions through a 100 nm track-etched membrane.

Vesicles to encapsulate RNA were prepared using a resuspension solution containing the species to be encapsulated; extruded vesicles were purified over a Sepharose 4B column in running buffer containing vesicles of identical composition to the mixture to be purified. Vesicle-containing fractions were identified by emission of the fluorescein tag on encapsulated oligonucleotides ($\lambda_{ex}$ = 495 nm and $\lambda_{em}$ = 520 nm).

The composition of the MA/GMO vesicles was 66.7 mM/33.3 mM and the composition of the MA/GMO/DOPA vesicles was 60 mM/30 mM/10 mM. All vesicles were always incubated with tumbling.

**Vesicle growth.** Vesicle growth was performed by mixing MA/GMO/DOPA vesicles with MA/GMO vesicles (20 equiv., 4 vol. at 5× lipid concentration), several inversions of the vial containing the vesicles and tumbling for 3 h before subsequent manipulations. This incubation was sufficient to allow 90–95% volume equilibration (Supplementary Fig. 6).

Where vesicle growth was monitored by Förster resonance energy transfer (FRET), FRET is reported as $F_d/F_a$, or the ratio of the donor (NBD) fluorescence ($\lambda_{em}$ = 530 nm) to the acceptor (rhodamine) fluorescence ($\lambda_{em}$ = 586 nm) with $\lambda_{ex}$ = 430 nm. Lipids labelled with these dyes were present at an initial concentration of 0.2 mol% total dye (that is, 0.1% each lipid) and changes in surface area due to membrane growth were calculated from a standard curve of lipid dye concentration in the membrane, relative to $F_d/F_a$ (Supplementary Fig. 5). Fluorescence measurements of vesicles were read at the bottom of the plate to minimize scattering.

**Hammerhead reactions.** Except where specified, hammerhead reactions were performed in 250 mM tris-HCl, pH 8, with 4 mM $MgCl_2$. Reaction mixtures were generated by mixing all reaction components except **HH-A** and $MgCl_2$ to generate **HH-B**-inhibitor complexes; **HH-A** was then added, giving a reaction mixture containing the highest used **HH-A/HH-B** concentration (that is, 10 μM, or 1 μM for encapsulation mixtures). An inhibited ribozyme that could be activated to the same extent by dilution could also be generated from preformed **HH-A/HH-B**, suggesting that an equilibrium mixture of **HH-A/HH-B**/inhibitors is present in these reactions (Supplementary Fig. 4). Reaction mixtures were then diluted or encapsulated in vesicles (as described above) as desired, and the cleavage reaction was initiated by the addition of a 10× (that is, 40 mM) solution of $MgCl_2$.

Reaction volumes were 10 μl for unencapsulated 10 μM and 1 μM reactions and 100 μl for unencapsulated 0.1 μM reactions. Encapsulated reactions were prepared in 100 μl volumes. Following column purification, this volume increased to ~750–900 μl. Vesicles were purified in running buffer of identical lipid concentration, ensuring that the internal volume of the vesicles (and, therefore, concentrations of encapsulated RNAs) remained constant during initial purification. A typical sample was 120 μl, mixed with four volumes of vesicles at 5× (that is, 500 mM total lipid) concentration. Vesicles undergoing growth were mixed with vesicles lacking phospholipid; those not undergoing growth were subjected to a dummy treatment of mixing with vesicles of identical composition. Encapsulated reactions were stopped by vesicle lysis with 1% Triton X-100, followed by ethanol precipitation overnight at –20 °C (300–350 μl of vesicle sample was typically precipitated), three additional washes with 100 μl 70% ethanol and resuspension in 10 μl 8 M urea, 1× TBE, which was used to load the sample on gels for analysis. The precipitation and wash procedure gave identical recovery efficiencies for both **HH-A** and its cleavage product (Supplementary Fig. 8).

Non-encapsulated reactions were stopped at the desired time points by the addition of an aliquot (1–10 μl) of the reaction mixture to gel loading buffer containing 8 M urea, 1× TBE and 20 mM additional EDTA (10–99 μl), yielding 50–100 nM **HH-A/HH-B** in loading buffer. The resulting samples were loaded directly (that is, without ethanol precipitation) in 5–10 μl volumes containing 250–500 fmol end-labelled oligonucleotide.

Reactions were analysed by 20 or 15% polyacrylamide gel electrophoresis (PAGE) and imaged on a Typhoon phosphorimager by monitoring the fluorescence of the 5′-fluorescein tag on **HH-A**; all other strands employed were not end-labelled. A green (532 nm) laser was employed as the excitation source and a 526 nm short-pass filter as the emission filter. Gel integrations were performed with GelQuant.NET. An electropherogram showing **HH-A** (25 nt) and its cleavage product (19 nt) alongside a size marker ladder (10, 15, 20, 25, 30 ssRNA nt) is presented in Supplementary Fig. 9, demonstrating that the cleavage product is of the expected length.

Both the longest strand used (**HH-A**) and a fluorescently labelled DNA analogue of the shortest strand employed (**FAM-DNA-HH-I-3**) were retained within vesicles, even after growth and magnesium addition, over the experimental time course (Supplementary Fig. 10), demonstrating that the reaction takes place within the fatty acid vesicles.

Received 3 September 2015; accepted 4 February 2016; published online 14 March 2016

## References


1. Chen, I. A. & Szostak, J. W. A kinetic study of the growth of fatty acid vesicles. *Biophys. J.* **87,** 988–998 (2004).
2. Chen, I. A., Roberts, R. W. & Szostak, J. W. The emergence of competition between model protocells. *Science* **305,** 1474–1476 (2004).
3. Adamala, K. & Szostak, J. W. Competition between model protocells driven by an encapsulated catalyst. *Nature Chem.* **5,** 495–501 (2013).
4. Peterlin, P., Arrigler, V., Kogej, K., Svetina, S. & Walde, P. Growth and shape transformations of giant phospholipid vesicles upon interaction with an aqueous oleic acid suspension. *Chem. Phys. Lipids* **159,** 67–76 (2009).
5. Rogerson, M. L., Robinson, B. H., Bucak, S. & Walde, P. Kinetic studies of the interaction of fatty acids with phosphatidylcholine vesicles (liposomes). *Colloids Surf. B* **48,** 24–34 (2006).
6. Cheng, Z. & Luisi, P. L. Coexistence and mutual competition of vesicles with different size distributions. *J. Phys. Chem. B* **107,** 10940–10945 (2003).
7. Budin, I. & Szostak, J. W. Physical effects underlying the transition from primitive to modern cell membranes. *Proc. Natl Acad. Sci. USA* **108,** 5249–5254 (2011).
8. Stano, P. & Luisi, P. L. Achievements and open questions in the self-reproduction of vesicles and synthetic minimal cells. *Chem. Commun.* **46,** 3639–3653 (2010).
9. Walde, P., Umakoshi, H., Stano, P. & Mavelli, F. Emergent properties arising from the assembly of amphiphiles. Artificial vesicle membranes as reaction promoters and regulators. *Chem. Commun.* **50,** 10177–10197 (2014).
10. Uhlenbeck, O. C. A small catalytic oligoribonucleotide. *Nature* **328,** 596–600 (1987).
11. Chen, I. A., Salehi-Ashtiani, K. & Szostak, J. W. RNA catalysis in model protocell vesicles. *J. Am. Chem. Soc.* **127,** 13213–13219 (2005).
12. Szostak, J. W. An optimal degree of physical and chemical heterogeneity for the origin of life? *Phil. Trans.R. Soc. B* **366,** 2894–2901 (2011).
13. Wochner, A., Attwater, J., Coulson, A. & Holliger, P. Ribozyme-catalyzed transcription of an active ribozyme. *Science* **332,** 209–212 (2011).
14. Johnston, W. K., Unrau, P. J., Lawrence, M. S., Glasner, M. E. & Bartel, D. P. RNA-catalyzed RNA polymerization: accurate and general RNA-templated primer extension. *Science* **292,** 1319–1325 (2001).
15. Soukup, G. A. & Breaker, R. R. Relationship between internucleotide linkage geometry and the stability of RNA. *RNA* **5,** 1308–1325 (1999).
16. Adamala, K., Engelhart, A. E. & Szostak, J. W. Generation of functional RNAs from inactive oligonucleotide complexes by non-enzymatic primer extension. *J. Am. Chem. Soc.* **137,** 483–489 (2015).
17. Mattick, J. S. & Makunin, I. V. Non-coding RNA. *Human Molecular Genetics* **15 (Spec No. 1),** R17–R29 (2006).
18. Le Novère, N. MELTING, computing the melting temperature of nucleic acid duplex. *Bioinformatics* **17,** 1226–1227 (2001).
19. Dumousseau, M., Rodriguez, N., Juty, N. & Le Novère, N. MELTING, a flexible platform to predict the melting temperatures of nucleic acids. *BMC Bioinformatics* **13,** 101 (2012).


## Acknowledgements

The authors thank K.A. Björkbom, T. Walton, N. Kamat, C. Hentrich, L. Jin and other Szostak laboratory members for discussions. This work was supported in part by NASA Exobiology grant NNX11AD56G to J.W.S. and a grant (290363) from the Simons Foundation to J.W.S. A.E.E. was supported by an appointment to the NASA Postdoctoral Program, administered by Oak Ridge Associated Universities through a contract with

NASA, and by a Tosteson Fellowship from the Massachusetts General Hospital Executive Committee on Research. J.W.S. is an Investigator of the Howard Hughes Medical Institute.

## Author contributions

A.E.E., K.P.A. and J.W.S. designed experiments, analysed data and wrote the manuscript. A.E.E. and K.P.A. performed experiments. A.E.E. and K.P.A. contributed equally to this work.

## Additional information

Supplementary information is available in the online version of the paper. Reprints and permissions information is available online at www.nature.com/reprints. Correspondence and requests for materials should be addressed to J.W.S.

## Competing financial interests

The authors declare no competing financial interests.